

See discussions, stats, and author profiles for this publication at: <https://www.researchgate.net/publication/273784203>

Role of Bromide in Hydrogen Peroxide Oxidation of CTAB-Stabilized Gold Nanorods in Aqueous Solutions

ARTICLE *in* LANGMUIR · MARCH 2015

Impact Factor: 4.46 · DOI: 10.1021/acs.langmuir.5b00137 · Source: PubMed

CITATIONS

4

READS

71

4 AUTHORS, INCLUDING:



Jian Wu

Shanghai Jiao Tong University

12 PUBLICATIONS 22 CITATIONS

[SEE PROFILE](#)

Role of Bromide in Hydrogen Peroxide Oxidation of CTAB-Stabilized Gold Nanorods in Aqueous Solutions

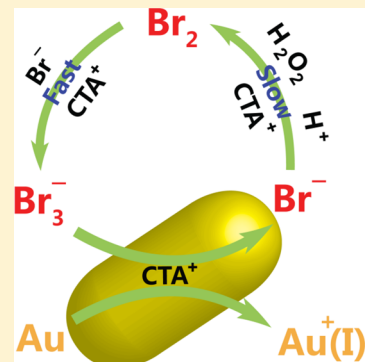
Qiannan Zhu,^{†,‡} Jian Wu,[†] Junwei Zhao,[†] and Weihai Ni*,[†]

[†]Division of i-Lab & Key Laboratory for Nano-Bio Interface Research, Suzhou Institute of Nano-Tech & Nano-Bionics, Chinese Academy of Sciences, Suzhou, Jiangsu 215123, China

[‡]Nano Science and Technology Institute, University of Science and Technology of China, 166 Ren'ai Road, Suzhou, Jiangsu 215123, China

S Supporting Information

ABSTRACT: In recent years hydrogen peroxide has often been used as the oxidizing agent to tune the resonance wavelength of gold nanorods (AuNRs) through anisotropic shortening in the presence of cetyltrimethylammonium bromide (CTAB). However, a complete picture of the reaction mechanism remains elusive. In this work, we present a systematic study on the mechanism of the AuNR oxidation by revealing the important role of bromide. Hydrogen peroxide slowly oxidizes bromide into elemental bromine. The latter two form tribromide, which exhibits a characteristic 272 nm absorption peak. The peak intensity, representing the concentration of tribromide, is found to have a linear correlation with the oxidation rate of AuNRs. Tribromide approaches AuNRs through conjugating strongly with CTA cationic micelles, which leads to the oxidation occurring on the surface of AuNRs. In contrast, the CTA micelles protect AuNRs from the direct oxidation by hydrogen peroxide. Our findings are believed to provide new insights into the reaction mechanism occurring in the relevant CTAB–AuNR systems, which can be important for understanding the principles governing the reaction dynamics.



INTRODUCTION

Excitation of free electron oscillations in metallic nanostructures gives rise to rich plasmonic properties which are favorable in many applications including plasmon-enhanced spectroscopy,¹ plasmonic sensing,² light harvesting,^{3–5} photothermal therapy,⁶ and metamaterials.⁷ The resonance wavelength is a crucial factor to be considered in the applications, which is closely related with the composite, shape, size, and environment of the nanostructure.⁸ As a typical type of anisotropic metallic nanostructure, gold nanorods (AuNRs) exhibit transverse and longitudinal surface plasmon resonances, corresponding to electron oscillations perpendicular and parallel to the long axis, respectively. The longitudinal surface plasmon resonance wavelength (LSPRW) is mainly determined and can be tuned from the visible to near-infrared region by the aspect ratio, the ratio between the long and short axes.^{9–12} Thanks to this tunable resonance wavelength, AuNRs are more advantageous than their spherical counterparts. The aspect ratio of AuNRs can be roughly varied by changing the dosage of the reaction reagents during the synthesis process of the seed-mediated growth.^{9,11} However, the possibility of controlling the aspect ratio of AuNRs during the growth process is rather limited mainly because the yield is also affected at the same time. Resizing after growth through oxidation or overgrowth is therefore much more preferable for tailoring the plasmonic properties.

Many efforts have been made to change the morphology of gold through oxidation and understand the oxidation

mechanism.¹³ For instance, cyanide dissolving gold in the presence of oxygen has long been used in the extraction and recovery of gold from ores.¹⁴ In 1993, the mechanism of bulk gold dissolution with bromine has been systematically studied by Pesic et al.¹⁵ The anisotropic shortening of the AuNRs using cyanide was first performed by Jana et al.¹⁶ Rodriguez-Fernandez et al. developed an effective method that the AuNRs can be shortened using Au(III) as oxidation agent.¹⁷ Tsung et al. further demonstrated dissolved oxygen in an acidic solution can easily oxidize AuNRs at the tips by thermal treatment.¹² Copper ions,^{18,19} ferric ions,^{20,21} or nitrite²² can also be used to induce the oxidation of AuNRs at room temperature. Since its first use in AuNR oxidation in 2008,²³ hydrogen peroxide has been employed in many oxidation experiments.^{24–27} Moreover, hydrogen peroxide generated by glucose oxidase can induce the oxidation of noble metal nanoparticles, which has been employed for the development of colorimetric glucose biosensors.^{27–29} Hydrogen peroxide oxidation of AuNRs was usually performed in the presence of cetyltrimethylammonium bromide (CTAB), where CTA cations provide stability to the otherwise unstable Au(I) product as capping surfactants. The halide counterions of the surfactant (i.e., Br⁻) have also been proved critical in the oxidation of CTAB-stabilized gold nanoparticles.^{24,27,30} In the

Received: December 29, 2014

Revised: March 17, 2015



reaction the role of bromide ions is depicted as lowering the metal's redox potential through chemical adsorption.^{17,27}

The complete picture of the mechanism for such oxidation reactions, however, remains elusive. For example, if hydrogen peroxide attacks gold directly, its consuming should result in a decreasing reaction rate. On the contrary, an increasing oxidation rate is always observed.^{12,23} Therefore, a complete study on the oxidation mechanism is required to explain the contradiction. Herein, we present a study on the mechanism by revealing the important role of bromide. A systematic experimental study is presented for the reactions involving bromide, CTA cationic micelles, hydrogen peroxide, etc. Their interactions in the reactions are discussed in detail. The proposed mechanism is believed to provide new insights into the mechanism occurring in other related CTAB–AuNR systems, which can be important for understanding the principles governing the reaction dynamics.

EXPERIMENTAL SECTION

Chemicals and Instruments. Hydrogen tetrachloroaurate(III) trihydrate, silver nitrate, L-ascorbic acid, cetyltrimethylammonium chloride (CTAC), CTAB, and sodium bromide were obtained from Sigma-Aldrich. Sodium borohydride, hydrochloric acid, hydrogen peroxide (30 wt %), and elemental bromine were obtained from Sinopharm Chemical Reagent Co. Ltd. All of these reagents were used without any further purification. Solutions were prepared with deionized water (18.2 MΩ).

Transmission electron microscopy (TEM) analyses were performed on a Tecnai G2 F20 S-Twin field-emission transmission electron microscope. Extinction spectra were recorded on an Agilent Technologies Cary 60 UV–vis spectrophotometer equipped with a thermal static cell holder, using 1 cm path length quartz cuvettes.

Preparation of AuNRs. The AuNRs were prepared using the silver ion-assisted seed-mediated method.^{9,31} The seed solution was prepared by the addition of an aqueous HAuCl₄ solution (5 mL, 0.5 mM) into an aqueous CTAB solution (5 mL, 0.2 M) in a plastic tube. After the solution was mixed by inversion, a freshly prepared, ice-cold aqueous NaBH₄ solution (0.6 mL, 0.01 M) was diluted to 1 mL with water and was then injected to the Au(III)–CTAB solution under vigorous stirring (1200 rpm) for 2 min. The resultant CTAB-stabilized Au nanoparticle seed solution was kept at room temperature for 1 h before use. The growth solution was made by mixing HAuCl₄ (2 mL, 0.01 M) and AgNO₃ (0.4 mL, 0.01 M) with CTAB (40 mL, 0.1 M) in a plastic tube. HCl (0.8 mL, 1.0 M) was then added, followed by the addition of a freshly prepared ascorbic acid solution (0.32 mL, 0.1 M). The resultant solution was mixed, and then the seed solution (0.015 mL) was added. The reaction mixture was agitated by gentle inversion for 10 s and left undisturbed at least overnight. The LSPRW of the resulting nanorods in water is 732 nm. The AuNR dimensions measured from TEM were $(86.1 \pm 4.3) \times (29.2 \pm 1.7)$ nm, with an aspect ratio of 3.0 ± 0.2 . The prepared Au nanorods were centrifuged twice to remove the excessive CTAB, unreacted species, and byproducts in the aqueous solution followed by removal of the supernatant and redispersed into the same volume of deionized water.

Oxidation of AuNRs Using H₂O₂. The oxidation of AuNRs using H₂O₂ was performed in two different procedures. The first one was commonly used in the previous reports.²³ To be specific, four concentrated AuNR aqueous solutions containing CTAB and HCl were incubated at 55 °C for 30 min, and then various volumes of H₂O₂ solution were added to obtain 5, 10, 15, and 20 mM H₂O₂. The final volume of the solutions was controlled at the same 1 mL. The concentrations of CTAB and HCl in the final solutions were 100 and 20 mM, respectively. The oxidation started at the addition of H₂O₂. In the second procedure, reaction solutions containing CTAB, HCl, and H₂O₂ was incubated at 55 °C for 30 min, and then concentrated AuNR solution was added. The final concentrations of all the substances in the solution were kept the same as the first procedure. The oxidation started at the addition of AuNRs. Time evolution of the

extinction spectra of the AuNR solutions was recorded, and the rate of oxidation was calculated in wavelength shift per minute.

Effect of H₂O₂, CTAB, and HCl on the Absorption Peak of Br₃⁻ at 272 nm. To investigate the effect of H₂O₂ on the absorption peak of Br₃⁻ at 272 nm, various volumes of H₂O₂ solution were added into the solution containing CTAB and HCl, to obtain 0, 7, 14, 27, and 46 mM H₂O₂. The reaction was allowed to proceed at 55 °C for 30 min while being monitored using UV–vis spectroscopy. Similarly, the effect of CTAB was studied by controlling its concentration at 0, 14, 50, and 100 mM. The effects of CTA⁺ and Br⁻ on the 272 nm absorption peak were further studied by replacing CTAB with CTAC and NaBr, respectively. To study the effect of HCl, the reaction solution containing no HCl was also investigated.

Effect of Br₃⁻ Peak Intensity on the Oxidation Rate of AuNRs. With the increase of the incubation time, the Br₃⁻ absorption peak at 272 nm exhibited by the reaction solution containing CTAB, HCl, and H₂O₂ started to appear and gradually increased in intensity. The incubation was performed at 45 °C. When the peak height reached a certain value, 0.25 mL of concentrated AuNR solution was added to 0.75 mL of the reaction solution to start the oxidation. The final concentrations of CTAB, HCl, and H₂O₂ were 0.1 M, 20 mM, and 20 mM, respectively. The procedure was repeated at different Br₃⁻ peak height (0.26, 0.46, 0.64, 0.84, 0.92, 1.06, 1.36, 1.50, and 1.70), and the oxidation rate was calculated as described above.

Effect of CTA⁺ and Br⁻ on the Oxidation Rate of AuNRs. To study the effect of Br⁻ on the oxidation rate of AuNRs, various amounts of NaBr solution were added to the mixed solutions containing CTAC, HCl, H₂O₂, and AuNRs, and hence 100, 75, 50, 30, 10, 5, and 1 mM Br⁻ were obtained. The final concentrations of CTAC, HCl, and H₂O₂ were 100, 20, and 150 mM, respectively. The temperature was controlled at 45 °C. For the analysis of CTA⁺ effect, 100, 75, 50, 30, 10, 5, and 1 mM CTAC were obtained, while NaBr was fixed at 0.1 M. Other reaction conditions were kept the same as described above, except that H₂O₂ was reduced to 30 mM when CTA⁺ was 1 mM for the convenience of the oxidation rate calculation.

Oxidation of AuNRs Using Br₂. The oxidation of AuNRs using Br₂ was carried out by adding different amount of Br₂ into reaction solution. One milliliter of as-synthesized AuNR solution was used without further purification treatment; 0.7, 1.0, 1.2, and 1.4 mM Br₂ were obtained. The oxidation rate gradually decreased when Br₂ was continuously consumed and became zero after reaction at 45 °C for 60 min. Those oxidized AuNRs with different aspect ratios were stable in several days without centrifugation.

RESULTS AND DISCUSSION

AuNRs were synthesized using the seed-mediated method.^{9,31} A representative transmission electron microscopy (TEM) image of the as-synthesized AuNRs is shown in Figure 1a. Their sizes are relatively uniform, with average dimension $(86.1 \pm 4.3) \times (29.2 \pm 1.7)$ nm, aspect ratio 3.0 ± 0.2 , and ensemble LSPRW at 732 nm. A commonly used oxidation procedure of AuNRs employing hydrogen peroxide as oxidation agent was introduced by our previous work.²³ The oxidation reaction is started when H₂O₂ is added to the reaction solution containing CTAB, HCl, and AuNRs. The average reaction rate is linearly dependent on the H₂O₂ concentration at a certain reaction temperature. In our experiments, reaction solution containing CTAB, HCl, and AuNRs was first heated up to 55 °C. As shown in Figure 1b, after the addition of H₂O₂ the longitudinal resonance peak of the AuNRs continuously performs a blue-shift and decreases in intensity. The blue-shift tends to be larger with the elapse of reaction time, suggesting the oxidation is accelerating (Figure 1c). This accelerating oxidation has been observed in many experiments.^{12,23}

Surprisingly, a distinct oxidation process was observed when the procedure was modified by incubating the reaction solution containing CTAB, HCl, and H₂O₂ at 55 °C for 30 min before

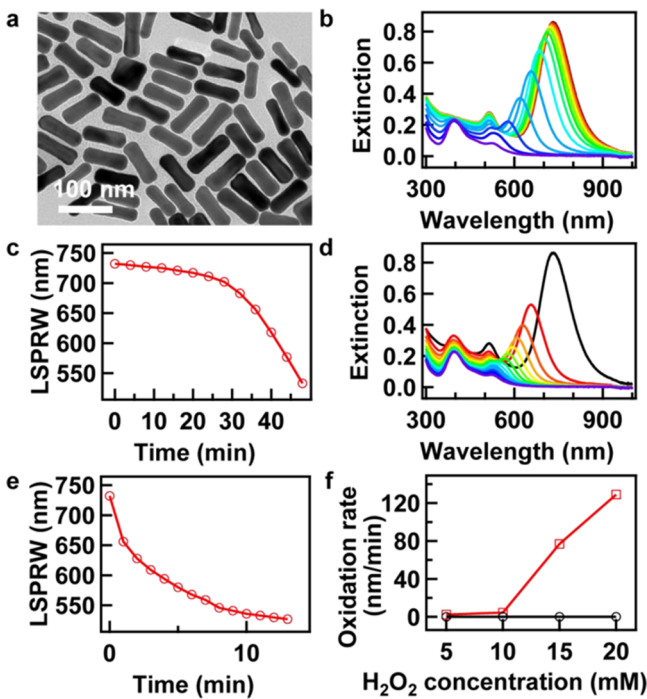


Figure 1. Comparison of AuNR oxidation between two procedures. (a) The TEM image of as-synthesized AuNRs. The average diameter, length, aspect ratio, and LSPRW of the AuNRs are 29.2 ± 1.7 nm, 86.1 ± 4.3 nm, 3.0 ± 0.2 , and 732 nm, respectively. (b) Time evolution of the AuNR extinction spectra. The spectra were recorded using the original procedure. The reaction solution containing CTAB, HCl, and AuNRs heated at 55 °C was added with H₂O₂. (c) The LSPRW vs reaction time. (d) Those for the modified procedure. The addition of AuNRs was performed after the incubation of the solution containing CTAB, HCl, and H₂O₂. H₂O₂ was 15 mM in (b) and (d). The spectra were acquired every 4 and 1 min in (b) and (d), respectively. (e) The LSPRW in (d) vs reaction time. (f) Oxidation rate plotted as a function of H₂O₂ concentration for the original (in black) and modified (in red) procedures. The oxidation rate was evaluated on the plasmon shift in the first several minutes of the reaction.

the addition of AuNRs. Other experimental conditions were kept the same as the original. Figure 1d shows the evolution of the extinction spectra of the AuNRs with the modified procedure. Upon the addition of AuNRs, as evidenced by the large blue-shift, the oxidation drastically takes place on the AuNRs in the first few minutes. The blue-shift decreases with time, indicating the slowing down of the oxidation reaction (Figure 1e), which is in contrast to the accelerating reaction observed without the incubation (Figure 1c). The two procedures were performed at other H₂O₂ concentrations and are shown in Figure S1 of the Supporting Information. Figure 1f shows the comparison of the initial rates between the two procedures which are evaluated based on the blue-shift in the first 4 and 1 min for the original and modified ones, respectively. The incubation resulted in orders of magnitude increase of the oxidation rate, suggesting another oxidant accumulating in the incubation period and taking effect.

In order to find out the oxidative substance that is responsible for the observed increase of the oxidation rate, the incubation of the mixture solution containing CTAB, HCl, and H₂O₂ at 45 °C was monitored using a UV-vis spectrophotometer. It was observed that an absorption peak at 272 nm started to appear and gradually increase in the spectrum (Figure 2a). As clearly shown in Figure 2b, the time-

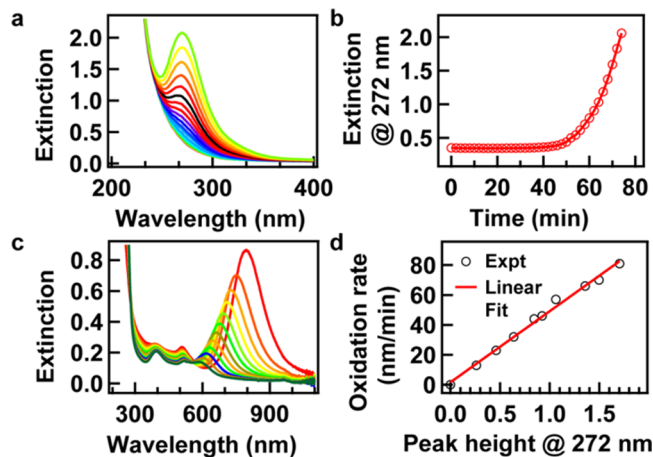
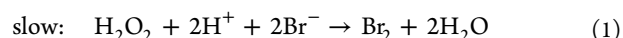


Figure 2. Appearance of absorption peak at 272 nm and its effect on the oxidation of AuNRs. (a) Time evolution of the absorption peak at 272 nm. (b) Peak height as a function of time. (c) Oxidation of AuNRs started by adding AuNRs to the reaction solution when its absorption peak height reaches 0.92. After the addition of AuNRs, the reaction solution contained 20 mM H₂O₂, 0.1 M CTAB, and 20 mM HCl. The spectra were acquired every 2 min at 45 °C for (a) and (c). (d) Oxidation rate versus the peak height at 272 nm. The oxidation rate shows a linear dependence on the peak height.

dependent intensity of the absorption peak exhibits a two-period process: the peak is hardly observable in the beginning 40 min but increases exponentially in the next 40 min.

It has been reported previously that hydrogen peroxide oxidizes bromide ion into elemental bromine in the presence of high concentrated H⁺.^{15,32,33} The bromide and bromine bind together to form tribromide, Br₃⁻.^{15,33} The reactions are shown as the following:

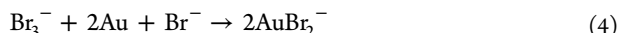


Equation 1 suggests the reaction is dependent on the concentrations of reagents on the left of the equation. A series of experiments were therefore performed by varying these concentrations. First, it is shown that the rising of the 272 nm absorption peak is positively related to the CTAB concentration (Figure S2). Second, the effect of CTA⁺ and Br⁻ was respectively investigated by replacing CTAB with CTAC and NaBr (Figures S3 and S4). According to the results, both CTA⁺ and Br⁻ are involved in the formation of the 272 nm absorption peak. The saturation intensity of the peak is determined by the Br⁻ concentration. Note that the presence of CTA⁺ actually slows down the rising of the peak (Figure S3f). Third, H₂O₂ concentration determines the reaction rate (Figure S5). Finally, the presence of H⁺ was also proved necessary for the reaction to occur (Figure S6). All these experimental facts are well consistent with eq 1, indicating the occurring of the reaction of eq 1.

To provide experimental proof for the reaction of eq 2 in the presence of CTAB, elemental bromine was purchased, diluted to 28 mM in aqueous solution, and mixed with 0.1 M CTAB solution, where Br₃⁻ can be formed by elemental bromine and the bromide of CTAB. As shown in Figure S7a, indeed, an absorption peak at 272 nm was instantly observed on the mixture solution. Attributing the characteristic 272 nm

absorption to Br_3^- is supported by many previous studies.^{34–37} The reaction of eq 2 is fast as the formation of Br_3^- is completed in hundreds of picoseconds.³⁸ Nevertheless, Br_3^- can be decomposed at 200 °C,³⁶ which may prevent characterizations involving high-energy excitations. Note that Br_3^- is slowly decomposed as evidenced by the decreasing intensity of the 272 nm peak in Figure S7a. A control experiment shows, when CTA^+ is absent, the decomposition process is much faster and the peak is also much lower, suggesting the presence of CTA^+ is important for stabilizing Br_3^- in aqueous solutions (Figure S7b). It can be explained that the formation of Br_3^- is favored by cationic micelles which interact very strongly with Br_3^- .³⁹ The conjugation or interaction is so strong that CTABr_3 can be isolated as a crystalline solid.³⁹ The solubility of Br_2 is also greatly enhanced in the presence of CTA^+ (Figure S7c) when compared with that in the absence of CTA^+ (Figure S7d). Nevertheless, CTA^+ cannot prevent the decomposition of Br_2 yet. It appears, in contrast with negatively charged Br_3^- , the neutral Br_2 does not have such affinity with CTA^+ . The enhancement of the solubility of some species by CTA^+ can also be seen in other reports where the CTA^+ micelles take effect.⁴⁰ The catalytic role of CTA^+ can therefore be described as (i) enhancement of the solubility of Br_2 by the micelle effect in the reaction of Br_2 generation and (ii) stabilization of Br_3^- by strong conjugation interactions. Finally, the overall reaction (eq 3) suggests the generation of Br_3^- is the consequence of the mixing H_2O_2 and CTAB , which is slowed down by the presence of CTA^+ .

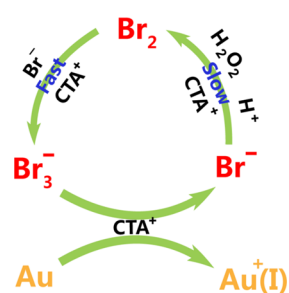
When AuNRs are added to the solution mixture containing Br_3^- , $\text{Au}(0)$ is oxidized to Au(I) by complexing into AuBr_2^- , while $\text{Br}(0)$ is reduced.¹⁵



To build the correlation between Br_3^- concentration and the oxidation rate of AuNRs, the reaction was performed by adding AuNRs to the mixture solutions with various 272 nm peak height. Upon addition of AuNRs, the extinction spectra were recorded (Figure 2c and Figure S8). As shown in Figure 2d, a linear dependence of the AuNR oxidation rate on the 272 nm peak height was found, which directly indicates Br_3^- exhibiting 272 nm absorption is responsible for the oxidation of AuNRs.

Therefore, the cycling of Br species involving eqs 1–4 is completed. Here we propose a mechanism shown in Scheme 1. Instead of directly oxidizing gold, hydrogen peroxide slowly oxidizes bromide ion into elemental bromine in the presence of CTA^+ . The bromide and bromine bind together to form Br_3^- where CTA^+ acts as a catalyst. Br_3^- acts as both oxidation and complex agents for dissolving Au into AuBr_2^- .

Scheme 1. Schematic Illustration of the Proposed Oxidation Mechanism



The proposed mechanism can be further proved by investigating the effect of either CTA^+ or Br^- concentrations on the overall AuNR oxidation rate. The effect of Br^- was investigated at two CTA^+ concentrations: 0.1 M and the critical micelle concentration (cmc) $\sim 1 \text{ mM}$ ⁴¹ (Figures S9 and S10). The oxidation rate decreases with the decrease of Br^- concentration. This observation is in good agreement with the previous report, where the effect of halides on the oxidation was investigated.²⁷ The oxidation rate becomes zero when Br^- is absent (Figure S9a), which gives a clear evidence that AuNRs cannot be directly oxidized by H_2O_2 . At both CTA^+ concentrations, the oxidation rate was found linearly dependent on Br^- concentration (Figure 3a), suggesting the reaction is

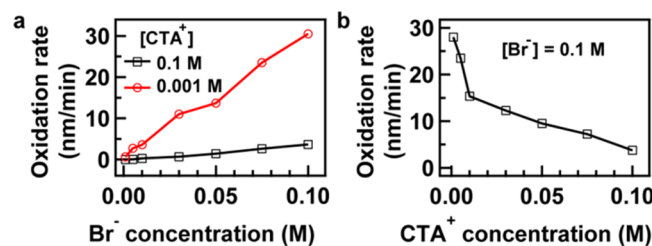


Figure 3. Effect of Br^- and CTA^+ concentrations on the oxidation rate of AuNRs. (a) Oxidation rate as a function of Br^- concentration at 0.001 and 0.1 M CTA^+ . (b) Oxidation rate as a function of CTA^+ concentration at 0.1 M Br^- . H_2O_2 concentration was 30 mM, and the temperature was 45 °C.

first order in Br^- . On the other hand, the oxidation rate decreases with the increase of CTA^+ concentration (Figure S11), which is well consistent with the slowing down of the generation of Br_3^- by CTA^+ . Interestingly, the CTA^+ dependence exhibits linear relations in two regions separated by the cmc. In the region below cmc, the slope is much steeper, which can be related with the incomplete covering of CTAB on the surface of AuNRs.⁴² It is worth noting that we also performed oxidation experiments under CTA^+ concentrations below the cmc. Without exception, all the experiments show a blue-shifted LSPRW when AuNRs are still stable in the solution. At some extremely low concentrations, we observed the precipitation of AuNRs on the sidewall of the cuvette, together with gradual decrease of the extinction spectrum with no shift (data not shown). We believe the same precipitation has been observed in the previous work though without being noticed.²⁴

The mechanism is confirmed by adding various amounts of elemental bromine to CTAB solution of AuNRs and monitoring the oxidation. As shown in Figure 4a and Figure S12, the LSPR peak performed blue-shift with decreasing intensity when the Br_2 solution was added. Time-dependent LSPRW was plotted at various Br_2 concentrations in Figure 4b, which clearly shows the initial oxidation rate is decreasing with the decrease of Br_2 concentration (from bottom to top). The slowing down of the reaction resembles the one shown in Figure 1e, suggesting the same mechanism of the oxidation reaction. Note that an absorption peak of AuBr_4^- at 400 nm is found in the final spectrum in Figure 1d, while it is absent in Figure 4a. This means H_2O_2 can further oxidize AuBr_2^- to AuBr_4^- , while AuBr_2^- is the final product in the case of Br_2 . With the depletion of Br_2 , the oxidation eventually stopped at a certain LSPRW. The final LSPRW was determined by the initial concentration of Br_2 . In this way, AuNRs with precisely

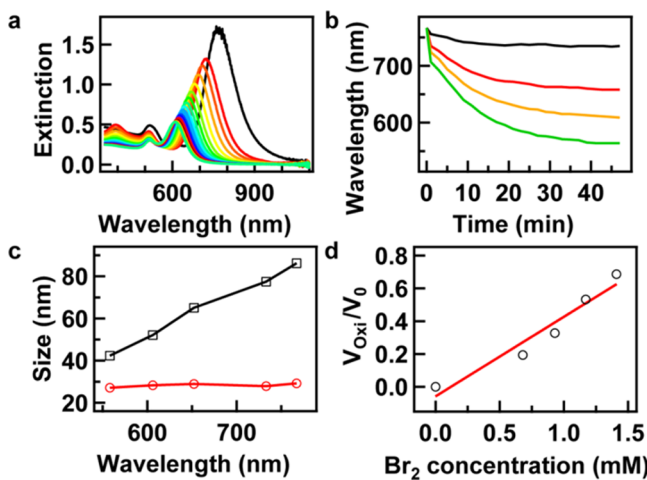


Figure 4. Oxidation of AuNRs using Br₂. (a) Time evolution of the extinction spectra of AuNRs acquired at 1.2 mM Br₂. Reaction temperature was 45 °C. Time interval is 2 min. (b) LSPRW of the oxidized AuNRs as a function of time. Br₂ concentrations are 0.7, 1.0, 1.2, and 1.4 mM from top to bottom, respectively. (c) Average length (squares, black) and diameter (circles, red) of the five AuNR samples as a function of the LSPRW. (d) Oxidized volume fraction of the AuNRs as a function of Br₂ concentration. The red line is a linear fit.

controlled LSPRW can be obtained. Figure S13 shows the TEM images of four AuNR samples after oxidation. These AuNRs are relatively stable in aqueous solutions, with their LSPRWs remaining unchanged for at least 1 week. Based on the TEM images, statistics show that the length of the oxidized AuNRs becomes smaller while the width is kept constant (Figure 4c). The oxidized volume fraction of the AuNRs was finally calculated and plotted as a function of Br₂ concentration, which exhibits a good linear dependence (Figure 4d).

Theoretically, hydrogen peroxide can directly oxidize gold simply considering the redox potential of H₂O₂/H⁺, H₂O (1.78 V vs the normal hydrogen electrode, NHE) and Au/Au⁺ (1.69 V vs NHE). However, actually zero oxidation rate is observed when Br⁻ concentration is zero (Figure S9a). In addition, it cannot be explained that oxidation rate is zero in the beginning a few minutes of the reaction when hydrogen peroxide concentration is high (Figure 1c). Instead, it is evidenced that tribromide with redox potential of Br₃⁻/Br⁻ (1.04 V vs NHE) can oxidize gold by complexing into AuBr₂⁻ because the complexing between the bromide ion and gold significantly decreases the redox potential of Au/Au⁺ from 1.69 to 0.95 V (vs NHE). The distinctive contrast between the oxidation behaviors of hydrogen peroxide and tribromide suggests a possible key mechanism governing the reaction in the aqueous solution. With excess Br⁻ from the CTAB present, bromine exists in the form of Br₃⁻. It has been evidenced in Figure S7a that Br₃⁻ conjugates with CTA⁺. Since CTA⁺ forms a protecting bilayer structure on the surface of AuNRs, the surface of AuNRs is believed directly accessible to Br₃⁻. Such kind of accessibility is not applicable for hydrogen peroxide, and therefore, direct oxidation is not possible. Alternatively, hydrogen peroxide oxidizes bromide into bromine. Bromine in the form of Br₃⁻ oxidizes Au to AuBr₂⁻, while the bromine is reduced to bromide ions. The cycling of bromide is thus accomplished (Scheme 1). Eventually, hydrogen peroxide further oxidizes AuBr₂⁻ to AuBr₄⁻. With the picture of this mechanism in mind, one can easily explain the observed increasing oxidation rate in Figure 1c. It is the Br₃⁻

concentration in the reaction solution that determines the oxidation rate, and the reaction is first order in Br₃⁻ (Figure 2d). Therefore, Br₃⁻ generation (Figure 2b) actually determines the behavior of the AuNR oxidation (Figure 1c). Indeed, a good agreement can be found. Of course, as the consuming of Br₃⁻ in AuNR oxidation is not negligible, time dependence of the oxidation rate does not exactly follow that of the Br₃⁻ generation.

In conclusion, we have performed a systematic study on the oxidation of AuNRs using hydrogen peroxide. On the basis of experimental observations, we propose a mechanism by exploring the important role of bromide. As evidenced by a series of experiments, instead of directly attacking gold, hydrogen peroxide actually slowly oxidizes bromide into elemental bromine. Tribromide formed by the two exhibits a characteristic 272 nm absorption peak, whose intensity was found linearly correlated with the oxidation rate. Tribromide approaches AuNRs through conjugating strongly with CTA cationic micelles, which leads to the oxidation occurring on the surface of AuNRs. In contrast, the CTA micelles protect AuNRs from the direct oxidation by hydrogen peroxide.

ASSOCIATED CONTENT

S Supporting Information

UV-vis extinction/absorption spectra and TEM images of AuNRs. This material is available free of charge via the Internet at <http://pubs.acs.org.org>.

AUTHOR INFORMATION

Corresponding Author

*E-mail: whni2012@sinano.ac.cn (W.N.).

Notes

The authors declare no competing financial interest.

ACKNOWLEDGMENTS

This work was financially supported by the National Natural Science Foundation of China (grants 21271181 and 21473240), Ministry of Science and Technology of the People's Republic of China (Intergovernmental S&T Cooperation Project, grant 2013-83-6-10), and Thousand Youth Talent Program of China.

REFERENCES

- Banholzer, M. J.; Millstone, J. E.; Qin, L. D.; Mirkin, C. A. Rationally designed nanostructures for surface-enhanced Raman spectroscopy. *Chem. Soc. Rev.* **2008**, *37* (5), 885–897.
- Stewart, M. E.; Anderton, C. R.; Thompson, L. B.; Maria, J.; Gray, S. K.; Rogers, J. A.; Nuzzo, R. G. Nanostructured plasmonic sensors. *Chem. Rev.* **2008**, *108* (2), 494–521.
- Silva, C. G.; Juarez, R.; Marino, T.; Molinari, R.; Garcia, H. Influence of excitation wavelength (UV or visible light) on the photocatalytic activity of titania containing gold nanoparticles for the generation of hydrogen or oxygen from water. *J. Am. Chem. Soc.* **2011**, *133* (3), 595–602.
- Brown, M. D.; Suteewong, T.; Kumar, R. S. S.; D'Innocenzo, V.; Petrozza, A.; Lee, M. M.; Wiesner, U.; Snaith, H. J. Plasmonic dye-sensitized solar cells using core-shell metal-insulator nanoparticles. *Nano Lett.* **2011**, *11* (2), 438–445.
- Linic, S.; Christopher, P.; Ingram, D. B. Plasmonic-metal nanostructures for efficient conversion of solar to chemical energy. *Nat. Mater.* **2011**, *10* (12), 911–21.
- Huang, X. H.; El-Sayed, I. H.; Qian, W.; El-Sayed, M. A. Cancer cell imaging and photothermal therapy in the near-infrared region by using gold nanorods. *J. Am. Chem. Soc.* **2006**, *128* (6), 2115–2120.

- (7) Yu, N. F.; Genevet, P.; Kats, M. A.; Aieta, F.; Tetienne, J. P.; Capasso, F.; Gaburro, Z. Light propagation with phase discontinuities: Generalized laws of reflection and refraction. *Science* **2011**, *334* (6054), 333–337.
- (8) Chen, H.; Shao, L.; Li, Q.; Wang, J. Gold nanorods and their plasmonic properties. *Chem. Soc. Rev.* **2013**, *42* (7), 2679–2724.
- (9) Nikoobakht, B.; El-Sayed, M. A. Preparation and growth mechanism of gold nanorods (NRs) using seed-mediated growth method. *Chem. Mater.* **2003**, *15* (10), 1957–1962.
- (10) Perez-Juste, J.; Liz-Marzan, L. M.; Carnie, S.; Chan, D. Y. C.; Mulvaney, P. Electric-field-directed growth of gold nanorods in aqueous surfactant solutions. *Adv. Funct. Mater.* **2004**, *14* (6), 571–579.
- (11) Jana, N. R.; Gearheart, L.; Murphy, C. J. Seed-mediated growth approach for shape-controlled synthesis of spheroidal and rod-like gold nanoparticles using a surfactant template. *Adv. Mater.* **2001**, *13* (18), 1389–1393.
- (12) Tsung, C.-K.; Kou, X.; Shi, Q.; Zhang, J.; Yeung, M. H.; Wang, J.; Stucky, G. D. Selective shortening of single-crystalline gold nanorods by mild oxidation. *J. Am. Chem. Soc.* **2006**, *128* (16), 5352–5353.
- (13) Long, R.; Zhou, S.; Wiley, B. J.; Xiong, Y. J. Oxidative etching for controlled synthesis of metal nanocrystals: Atomic addition and subtraction. *Chem. Soc. Rev.* **2014**, *43* (17), 6288–6310.
- (14) Jeffrey, M. I.; Ritchie, I. M. The leaching and electrochemistry of gold in high purity cyanide solutions. *J. Electrochem. Soc.* **2001**, *148* (4), D29–D36.
- (15) Pesic, B.; Sergent, R. H. Reaction-mechanism of gold dissolution with bromine. *Metall. Trans. B* **1993**, *24* (3), 419–431.
- (16) Jana, N. R.; Gearheart, L.; Obare, S. O.; Murphy, C. J. Anisotropic chemical reactivity of gold spheroids and nanorods. *Langmuir* **2002**, *18* (3), 922–927.
- (17) Rodriguez-Fernandez, J.; Perez-Juste, J.; Mulvaney, P.; Liz-Marzan, L. M. Spatially-directed oxidation of gold nanoparticles by Au(III)-CTAB complexes. *J. Phys. Chem. B* **2005**, *109* (30), 14257–14261.
- (18) Wen, T.; Zhang, H.; Tang, X. P.; Chu, W. G.; Liu, W. Q.; Ji, Y. L.; Hu, Z. J.; Hou, S.; Hu, X. N.; Wu, X. C. Copper ion assisted reshaping and etching of gold nanorods: Mechanism studies and applications. *J. Phys. Chem. C* **2013**, *117* (48), 25769–25777.
- (19) Zhang, Z. Y.; Chen, Z. P.; Qu, C. L.; Chen, L. X. Highly sensitive visual detection of copper ions based on the shape-dependent SPR spectroscopy of gold nanorods. *Langmuir* **2014**, *30* (12), 3625–3630.
- (20) Guo, X.; Zhang, Q.; Sun, Y. H.; Zhao, Q.; Yang, J. Lateral etching of core-shell Au@metal nanorods to metal-tipped Au nanorods with improved catalytic activity. *ACS Nano* **2012**, *6* (2), 1165–1175.
- (21) Zou, R. X.; Guo, X.; Yang, J.; Li, D. D.; Peng, F.; Zhang, L.; Wang, H. J.; Yu, H. Selective etching of gold nanorods by ferric chloride at room temperature. *CrystEngComm* **2009**, *11* (12), 2797–2803.
- (22) Chen, Z. P.; Zhang, Z. Y.; Qu, C. L.; Pan, D. W.; Chen, L. X. Highly sensitive label-free colorimetric sensing of nitrite based on etching of gold nanorods. *Analyst* **2012**, *137* (22), 5197–5200.
- (23) Ni, W.; Kou, X.; Yang, Z.; Wang, J. Tailoring longitudinal surface plasmon wavelengths, scattering and absorption cross sections of gold nanorods. *ACS Nano* **2008**, *2* (4), 677–686.
- (24) Chandrasekar, G.; Mougin, K.; Haidara, H.; Vidal, L.; Gnecco, E. Shape and size transformation of gold nanorods (GNRs) via oxidation process: A reverse growth mechanism. *Appl. Surf. Sci.* **2011**, *257* (9), 4175–4179.
- (25) Ni, W. H.; Ambjornsson, T.; Apell, S. P.; Chen, H. J.; Wang, J. F. Observing plasmonic-molecular resonance coupling on single gold nanorods. *Nano Lett.* **2010**, *10* (1), 77–84.
- (26) Ni, W. H.; Ba, H. J.; Lutich, A. A.; Jackel, F.; Feldmann, J. Enhancing single-nanoparticle surface-chemistry by plasmonic overheating in an optical trap. *Nano Lett.* **2012**, *12* (9), 4647–4650.
- (27) Saa, L.; Coronado-Puchau, M.; Pavlov, V.; Liz-Marzan, L. M. Enzymatic etching of gold nanorods by horseradish peroxidase and application to blood glucose detection. *Nanoscale* **2014**, *6* (13), 7405–7409.
- (28) Xia, Y. S.; Ye, J. J.; Tan, K. H.; Wang, J. J.; Yang, G. Colorimetric visualization of glucose at the submicromole level in serum by a homogenous silver nanoprism-glucose oxidase system. *Anal. Chem.* **2013**, *85* (13), 6241–6247.
- (29) Liu, X.; Zhang, S. Y.; Tan, P. L.; Zhou, J.; Huang, Y.; Nie, Z.; Yao, S. Z. A plasmonic blood glucose monitor based on enzymatic etching of gold nanorods. *Chem. Commun.* **2013**, *49* (18), 1856–1858.
- (30) Praharaj, S.; Panigrahi, S.; Basu, S.; Pande, S.; Jana, S.; Ghosh, S. K.; Pal, T. Effect of bromide and chloride ions for the dissolution of colloidal gold. *J. Photochem. Photobiol. A* **2007**, *187* (2–3), 196–201.
- (31) Sau, T. K.; Murphy, C. J. Seeded high yield synthesis of short Au nanorods in aqueous solution. *Langmuir* **2004**, *20* (15), 6414–6420.
- (32) Bray, W. C.; Livingston, R. S. The catalytic decomposition of hydrogen peroxide in a bromine-bromide solution, and a study of the steady state. *J. Am. Chem. Soc.* **1923**, *45*, 1251–1271.
- (33) Jang, E.; Lim, E. K.; Choi, J.; Park, J.; Huh, Y. J.; Suh, J. S.; Huh, Y. M.; Haam, S. Br-assisted Ostwald ripening of Au nanoparticles under H_2O_2 redox. *Cryst. Growth Des.* **2012**, *12* (1), 37–39.
- (34) Katzin, L. I. Regularities in the absorption spectra of halides. *J. Chem. Phys.* **1955**, *23* (11), 2055–2060.
- (35) Milne, J. A Raman-spectroscopic study of the effect of ion-pairing on the structure of the triiodide and tribromide ions. *Spectrochim. Acta, Part A: Mol. Biomol. Spectrosc.* **1992**, *48* (4), 533–542.
- (36) Lin, M. Z.; Archirel, P.; Van-Oanh, N. T.; Muroya, Y.; Fu, H. Y.; Yan, Y.; Nagaishi, R.; Kumagai, Y.; Katsumura, Y.; Mostafavi, M. Temperature dependent absorption spectra of Br^- , Br^{2-} , and Br^{3-} in aqueous solutions. *J. Phys. Chem. A* **2011**, *115* (17), 4241–4247.
- (37) Kerenskaya, G.; Goldschleger, I. U.; Apkarian, V. A.; Janda, K. C. Spectroscopic signatures of halogens in clathrate hydrate cages. 1. Bromine. *J. Phys. Chem. A* **2006**, *110* (51), 13792–13798.
- (38) El Omar, A. K.; Schmidhammer, U.; Balcerzyk, A.; LaVerne, J.; Mostafavi, M. Spur reactions observed by picosecond pulse radiolysis in highly concentrated bromide aqueous solutions. *J. Phys. Chem. A* **2013**, *117* (11), 2287–2293.
- (39) Rubingh, D. N.; Holland, P. M. *Cationic Surfactants: Physical Chemistry*; Marcel Dekker, Inc.: New York, 1990.
- (40) Sun, Z.; Yang, Z.; Zhou, J.; Yeung, M. H.; Ni, W.; Wu, H.; Wang, J. A general approach to the synthesis of gold-metal sulfide core-shell and heterostructures. *Angew. Chem., Int. Ed.* **2009**, *48* (16), 2881–5.
- (41) Huang, X. R.; Yang, J. H.; Zhang, W. J.; Zhang, Z. Y.; An, Z. S. Determination of the critical micelle concentration of cationic surfactants - An undergraduate experiment. *J. Chem. Educ.* **1999**, *76* (1), 93–94.
- (42) Jana, N. R.; Gearheart, L. A.; Obare, S. O.; Johnson, C. J.; Edler, K. J.; Mann, S.; Murphy, C. J. Liquid crystalline assemblies of ordered gold nanorods. *J. Mater. Chem.* **2002**, *12* (10), 2909–2912.

Supporting information for

Role of Bromide in Hydrogen-Peroxide Oxidation of CTAB-Stabilized Gold Nanorods in Aqueous Solutions

Qiannan Zhu,^{1,2} Jian Wu,¹ Junwei Zhao,¹ Weihai Ni^{1,}*

1. Division of *i*-Lab & Key Laboratory for Nano-Bio Interface Research, Suzhou Institute of Nano-Tech & Nano-Bionics, Chinese Academy of Sciences, Suzhou, Jiangsu, 215123, China
2. Nano Science and Technology Institute, University of Science and Technology of China, 166 Ren'ai Road, Suzhou, Jiangsu 215123, China

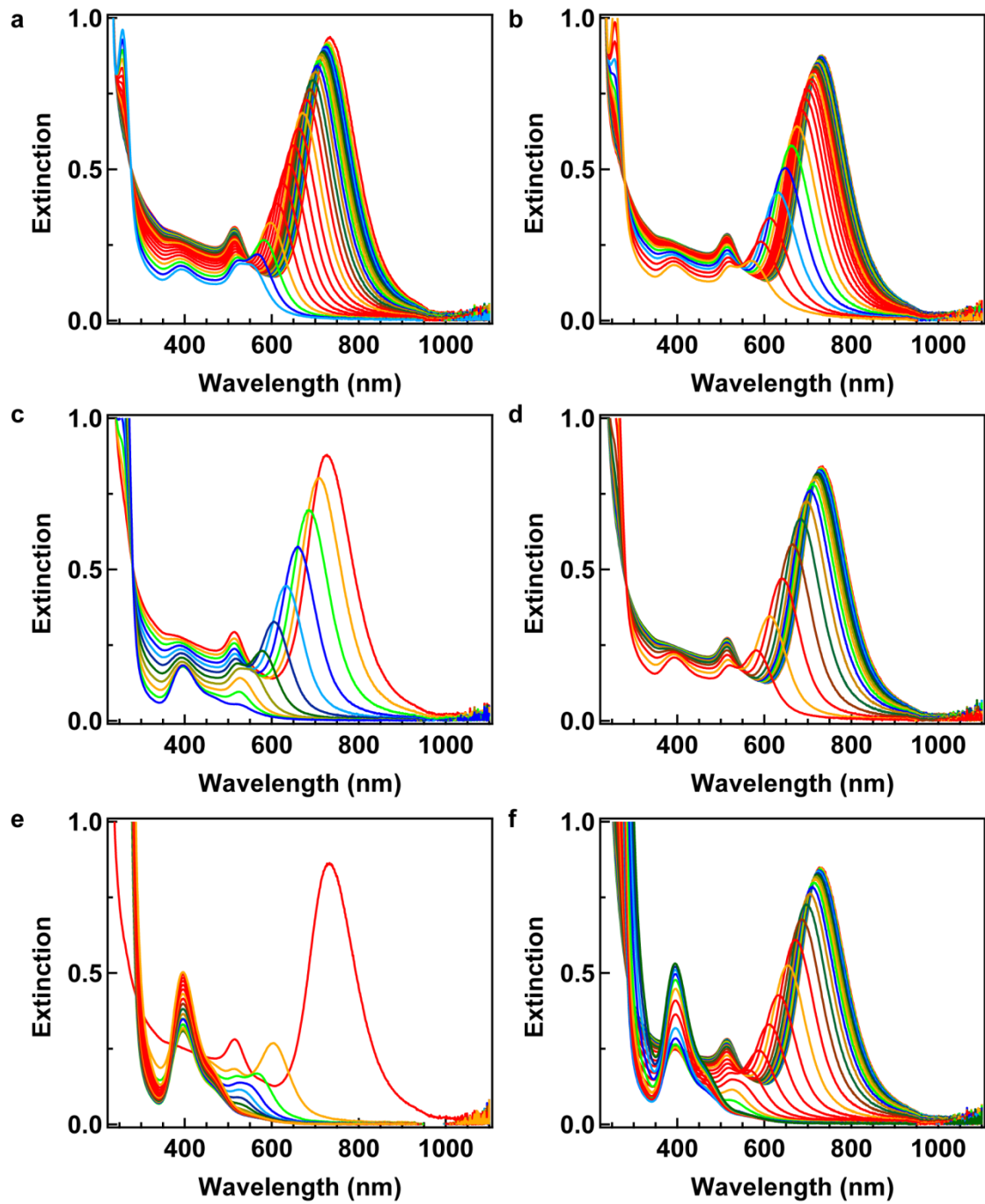


Figure S1. (a) Reaction solution containing CTAB, HCl, and H_2O_2 was incubated at 55 °C for 30 min and then AuNRs were added to start the oxidation. CTAB, HCl, and H_2O_2 concentrations were 0.1 M, 20 mM, and 5 mM in the final solution, respectively. (b) H_2O_2 was added after the incubation of the reaction solution containing CTAB, HCl, and AuNRs with the same concentration. (c) and (d) Those for 10 mM H_2O_2 . (e) and (f) Those for 20 mM

H_2O_2 . Time interval between spectra was 4 min for (a–d), 1 min for (e) and (f).

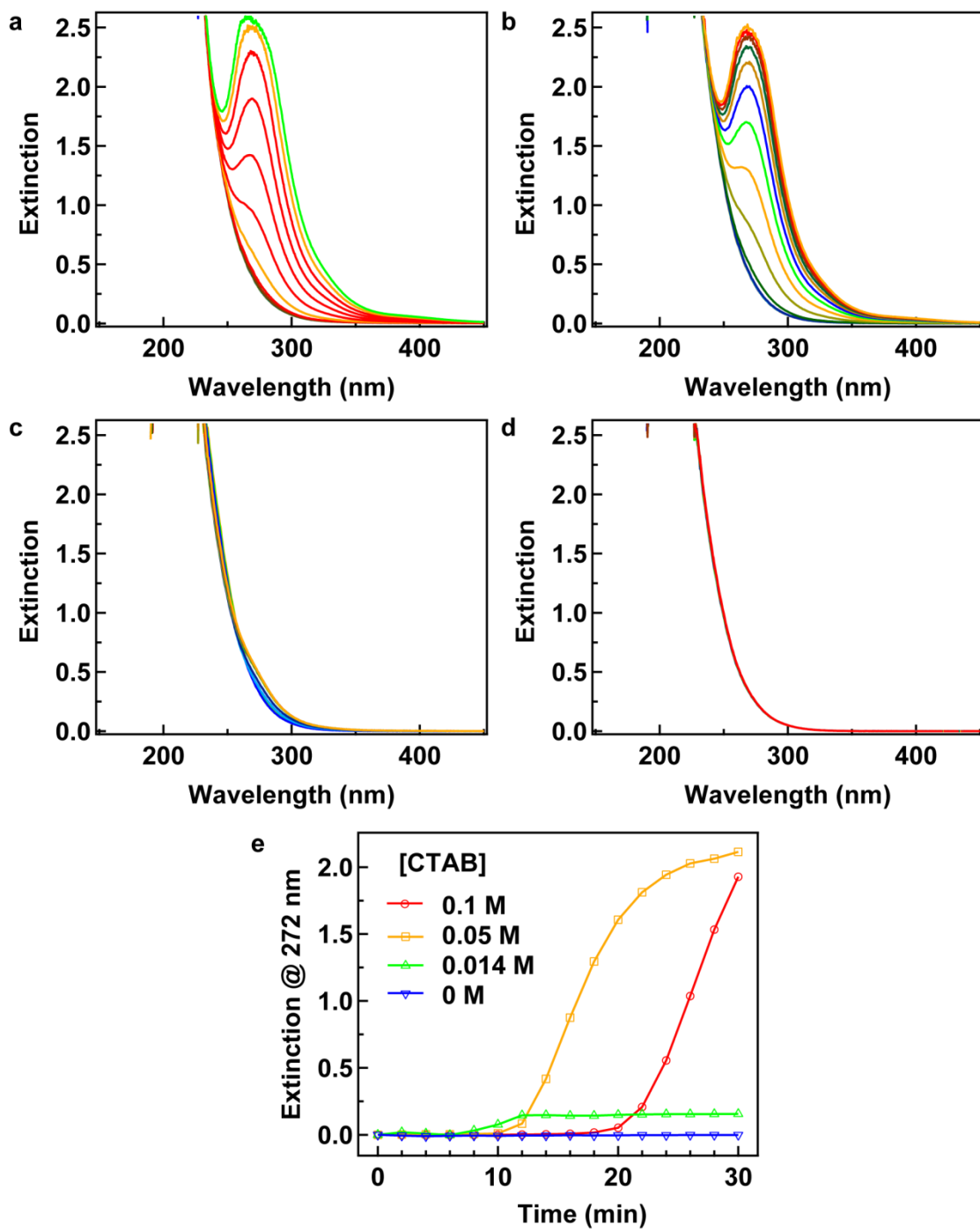


Figure S2. (a-d) Time evolution of the extinction spectra acquired at 0.1, 0.05, 0.014, and 0 M CTAB, respectively. The reaction solution contained 46 mM H₂O₂ and 27 mM HCl. The spectra were recorded every 2 min at 55 °C. (e) Peak height at 272 nm as a function of time at different concentrations of CTAB.

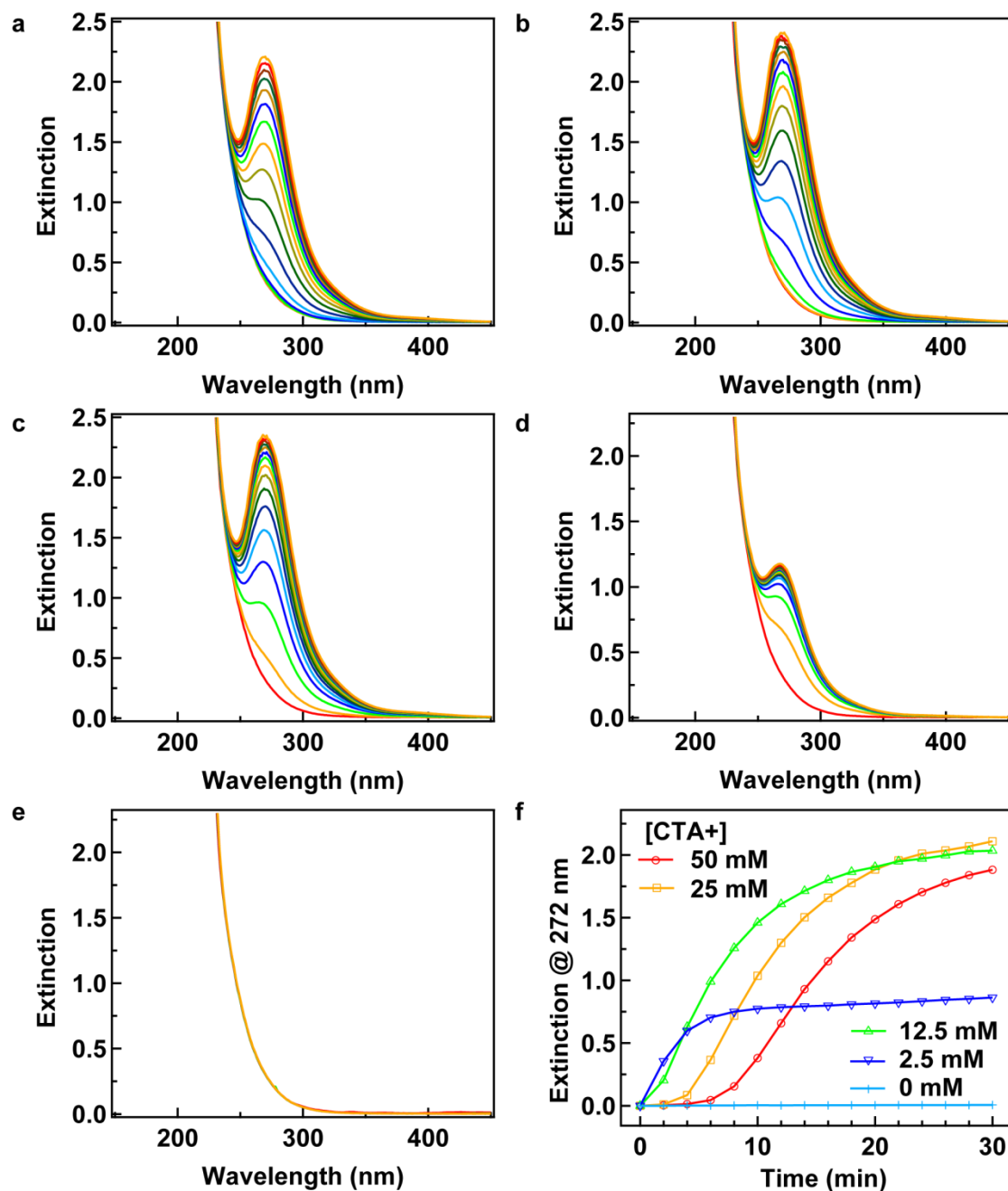


Figure S3. (a–e) Time evolution of the extinction spectra acquired at 50, 25, 12.5, 2.5, and 0 mM CTA⁺, respectively. The reaction solution contained 35 mM H₂O₂, 20 mM HCl, and 0.07 M Br⁻. The spectra were recorded every 2 min at 55 °C. (f) Peak height at 272 nm as a function of time at different concentrations of CTA⁺.

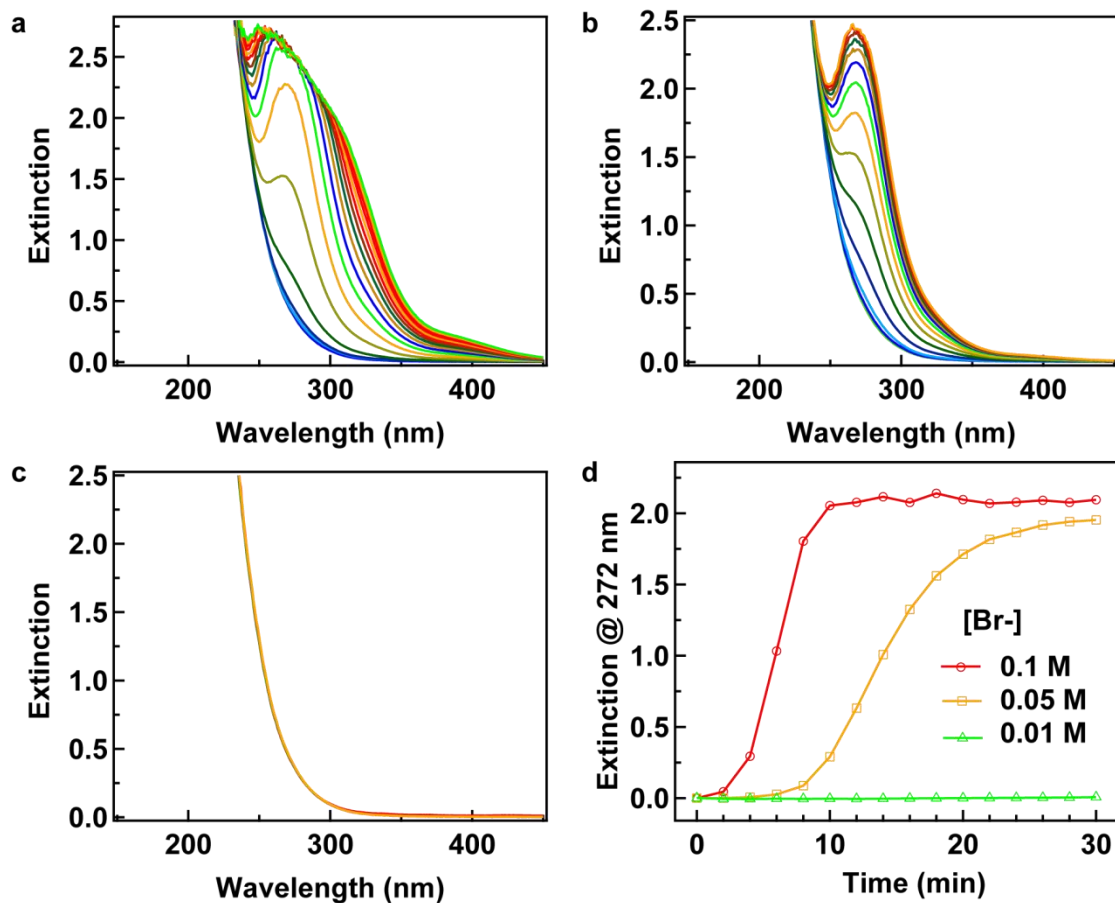


Figure S4. (a–c) Time evolution of the extinction spectra acquired at 0.1, 0.05, and 0.01 M Br⁻, respectively. The reaction solution contained 46 mM H₂O₂, 27 mM HCl, and 0.1 M CTA⁺. The spectra were recorded every 2 min at 55 °C. (d) Peak height at 272 nm as a function of time at different concentrations of Br⁻.

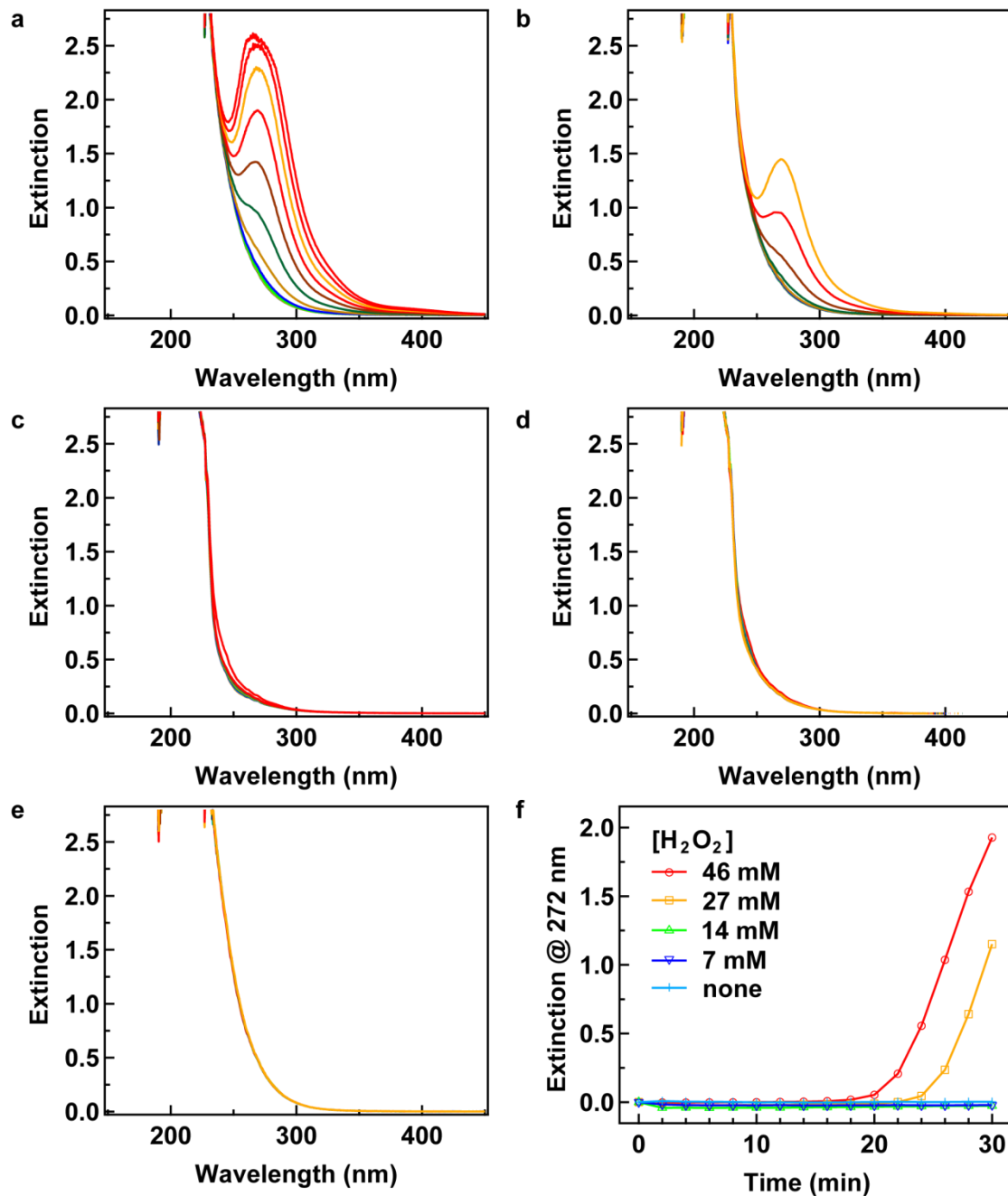


Figure S5. (a)–(e) Time evolution of the extinction spectra acquired at 46, 27, 14, 7, and 0 mM H₂O₂, respectively. The reaction solution contained 27 mM HCl, and 0.1 M CTAB. The spectra were recorded every 2 min at 55 °C. (f) 272-nm peak height as a function of time under different concentrations of H₂O₂.

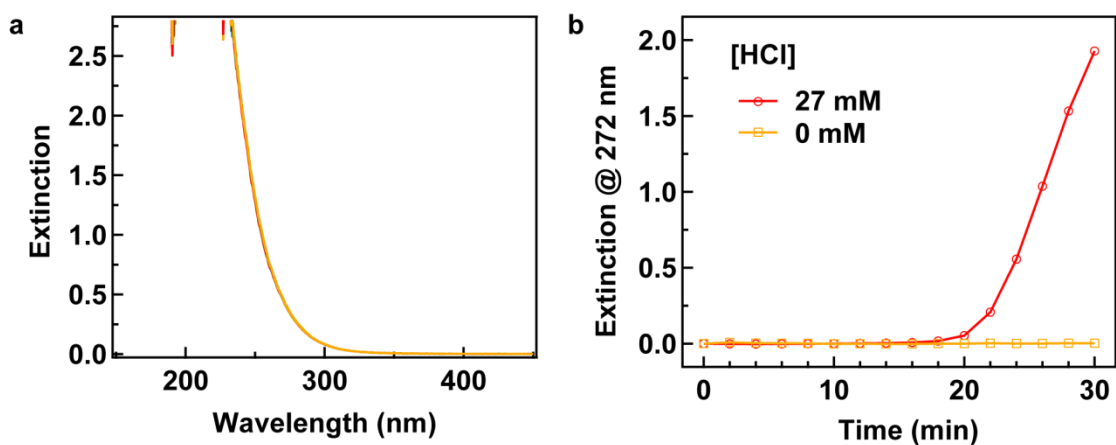


Figure S6. (a) Time evolution of the extinction spectra acquired without HCl. The reaction solution contained 0.1 M CTAB and 46 mM H_2O_2 . The spectra were recorded every 2 min at 55 °C. (b) 272-nm peak height as a function of time under different concentrations of HCl.

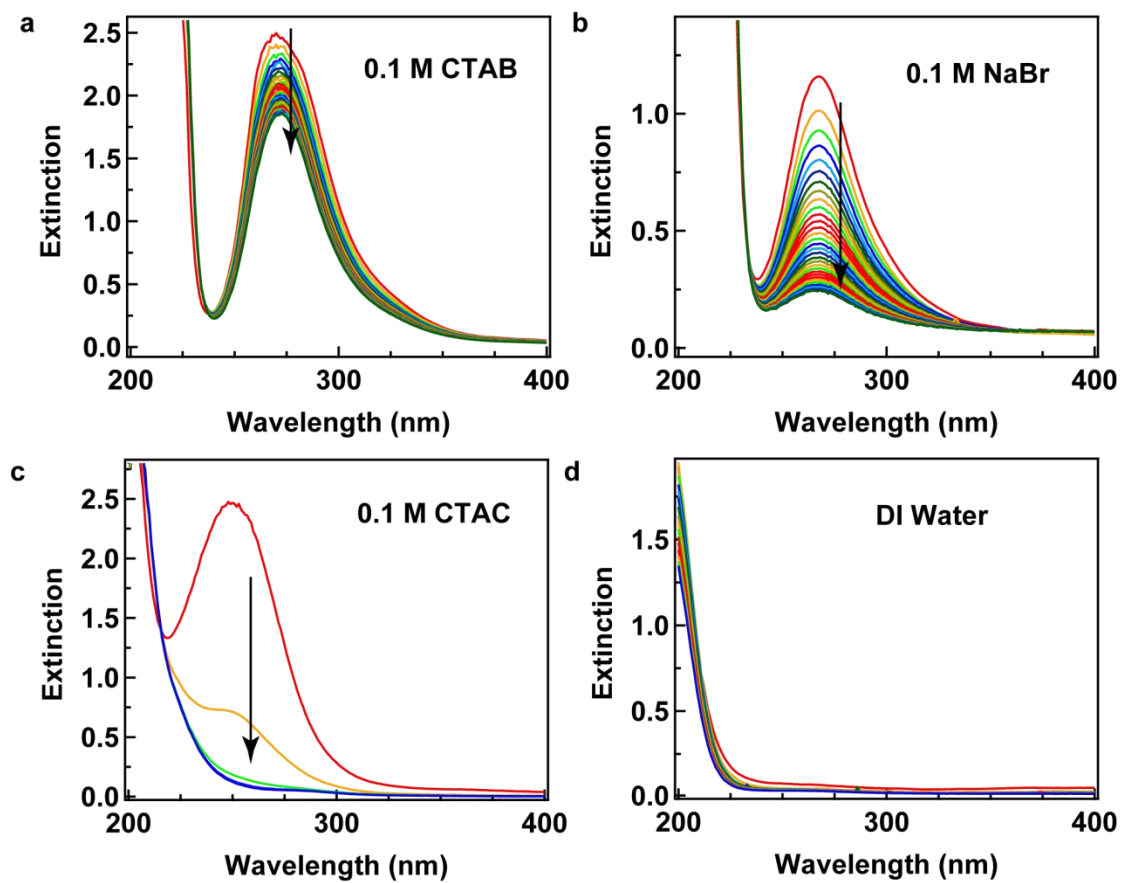


Figure S7. Extinction spectra acquired every 2 min after adding 10 μL of 28 mM Br_2 to 900 μL of (a) 0.1 M CTAB or (b) 0.1 M NaBr. 45 μL of 28 mM Br_2 was added to 900 μL of (c) 0.1 M CTAC or (d) deionized water. The reaction temperature was controlled at 55 °C. The absorption peak started to decrease upon the addition of Br_2 solution.

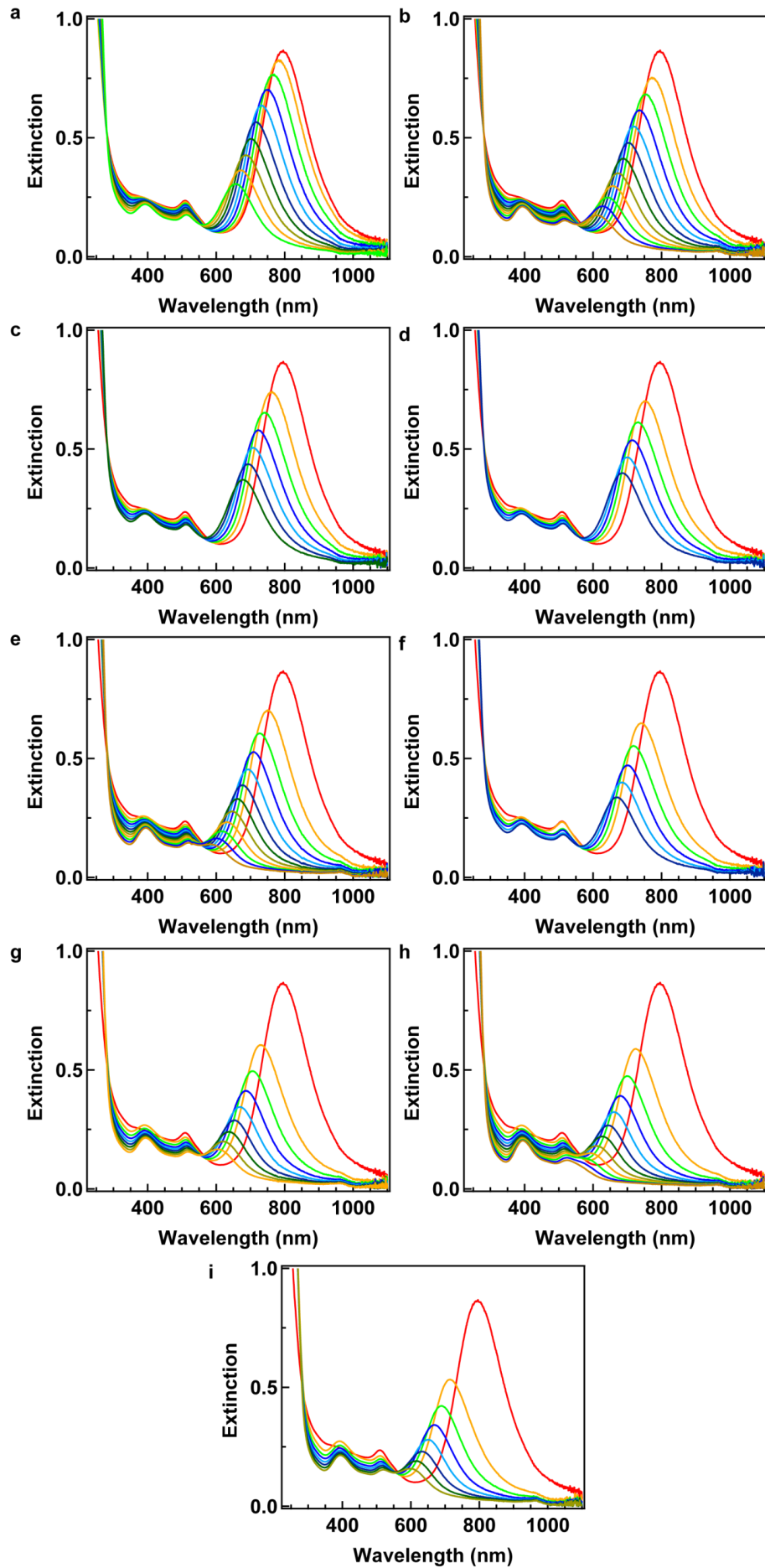


Figure S8. (a)–(h) Oxidation of AuNRs started by adding AuNRs to the reaction solution when its peak height reaches 0.26, 0.46, 0.64, 0.84, 1.06, 1.36, 1.50, and 1.70, respectively. The peak heights were obtained by subtracting the baseline from the 272 nm absorption spectra. The reaction solution contained 0.1 M CTAB, 20 mM HCl, and 20 mM H₂O₂. The spectra were recorded every 2 min at 45 °C.

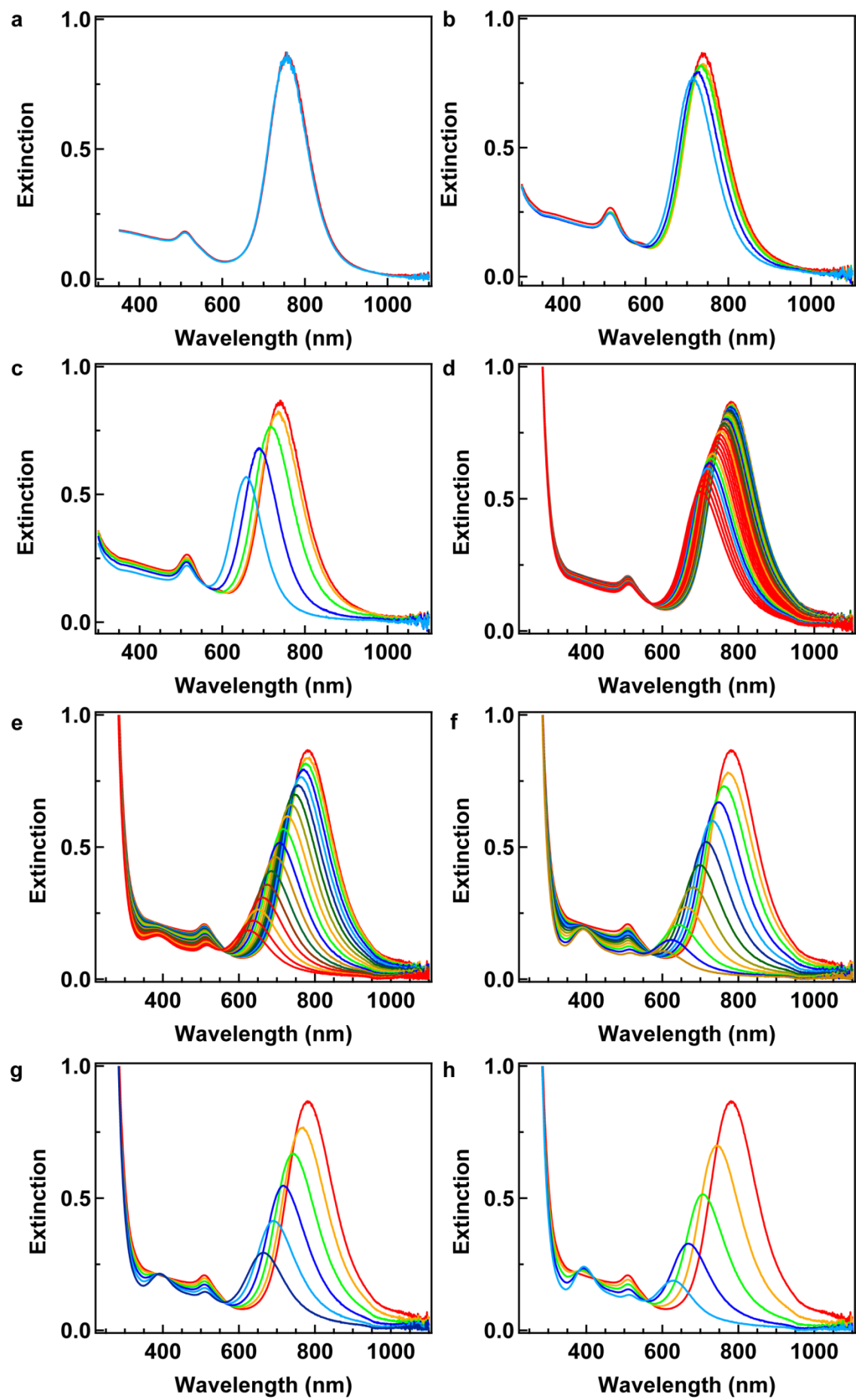


Figure S9. (a)–(h) Time evolution of the AuNR extinction spectra acquired at 0, 0.001, 0.005, 0.01, 0.03, 0.05, 0.075, and 0.1 M Br⁻, respectively. The reaction solution contained 20 mM HCl, 0.1 M CTA⁺, and 150 mM H₂O₂. The spectra were recorded every 1 hr for (a)–(c) and 2 min for others at 45 °C.

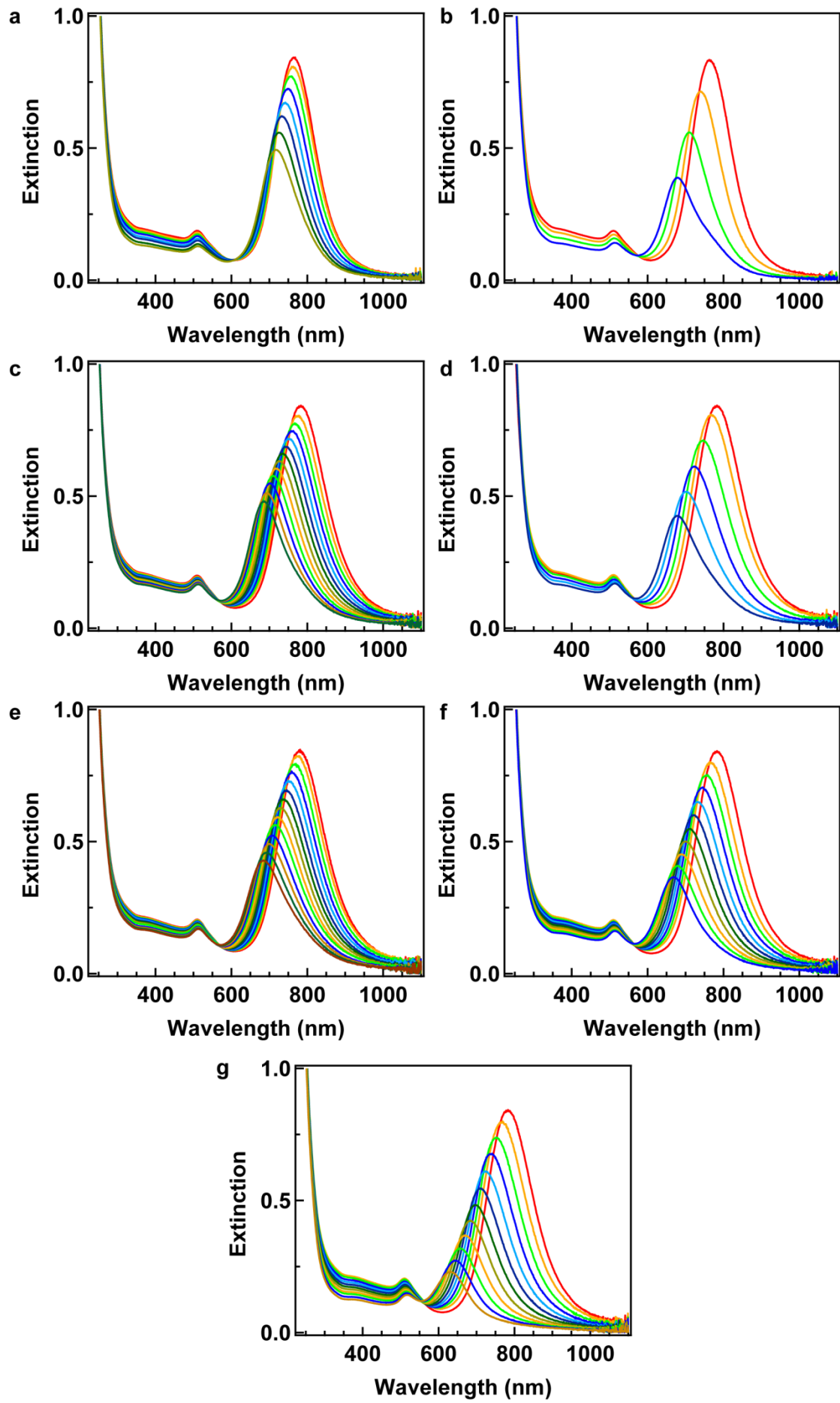


Figure S10. (a)–(h) Time evolution of the AuNR extinction spectra acquired at 0.001, 0.005, 0.01, 0.03, 0.05, 0.075, and 0.1 M Br⁻, respectively. The reaction solution contained 20 mM HCl, 0.001 M CTA⁺, and 30 mM H₂O₂. The spectra were recorded at 45 °C every 10 min for (a, b), 2 min for (c, d), and 0.5 min for (e, f, and g), respectively.

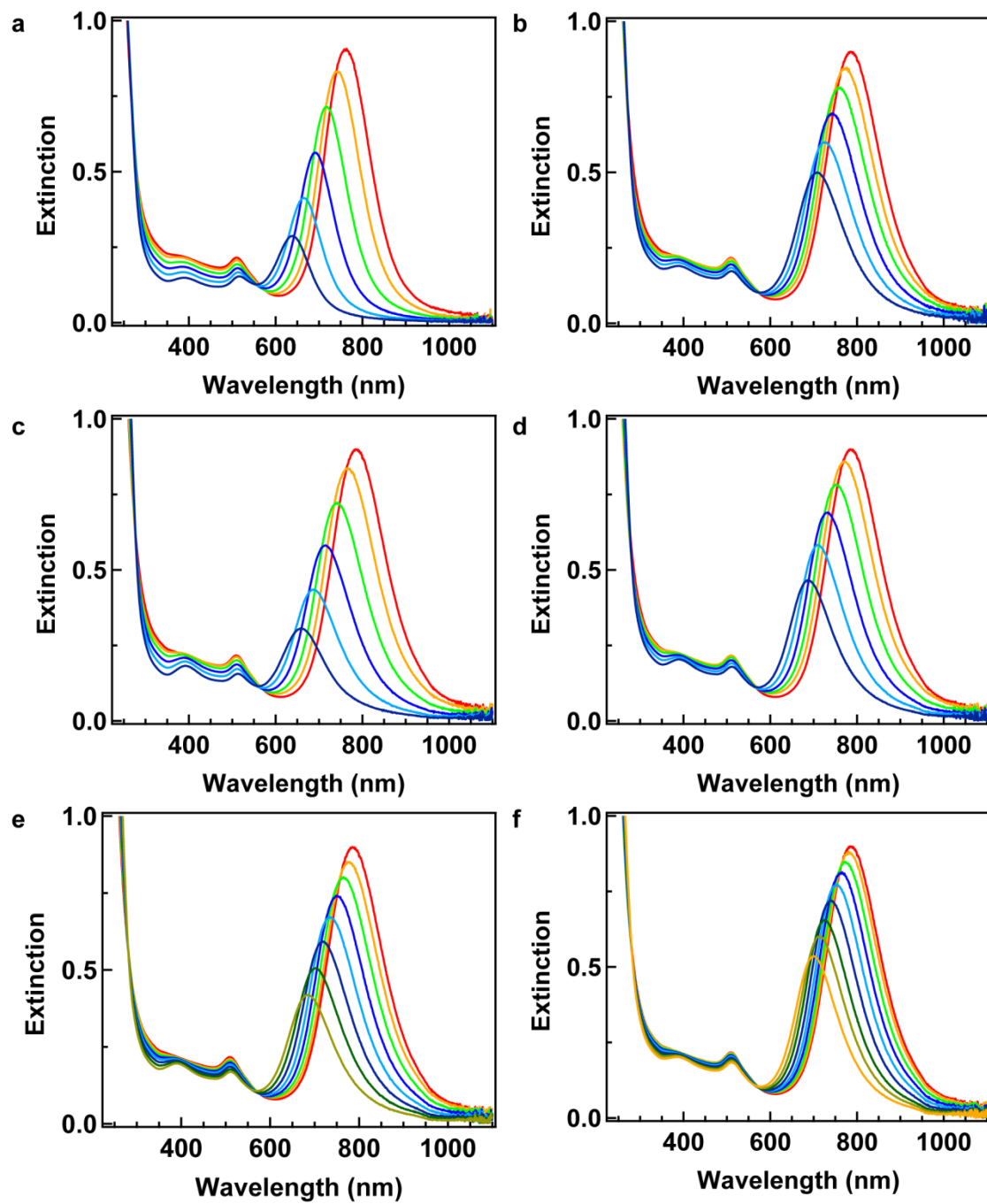


Figure S11. (a)–(f) Time evolution of the AuNR extinction spectra acquired at 0.005, 0.01, 0.03, 0.05, 0.075, and 0.1 M CTA^+ , respectively. The reaction solution contained 20 mM HCl, 0.1 M Br^- , and 30 mM H_2O_2 . The spectra were recorded at 45 °C every 1 min for (a, b) and 2 min for (c, d, e, and f).

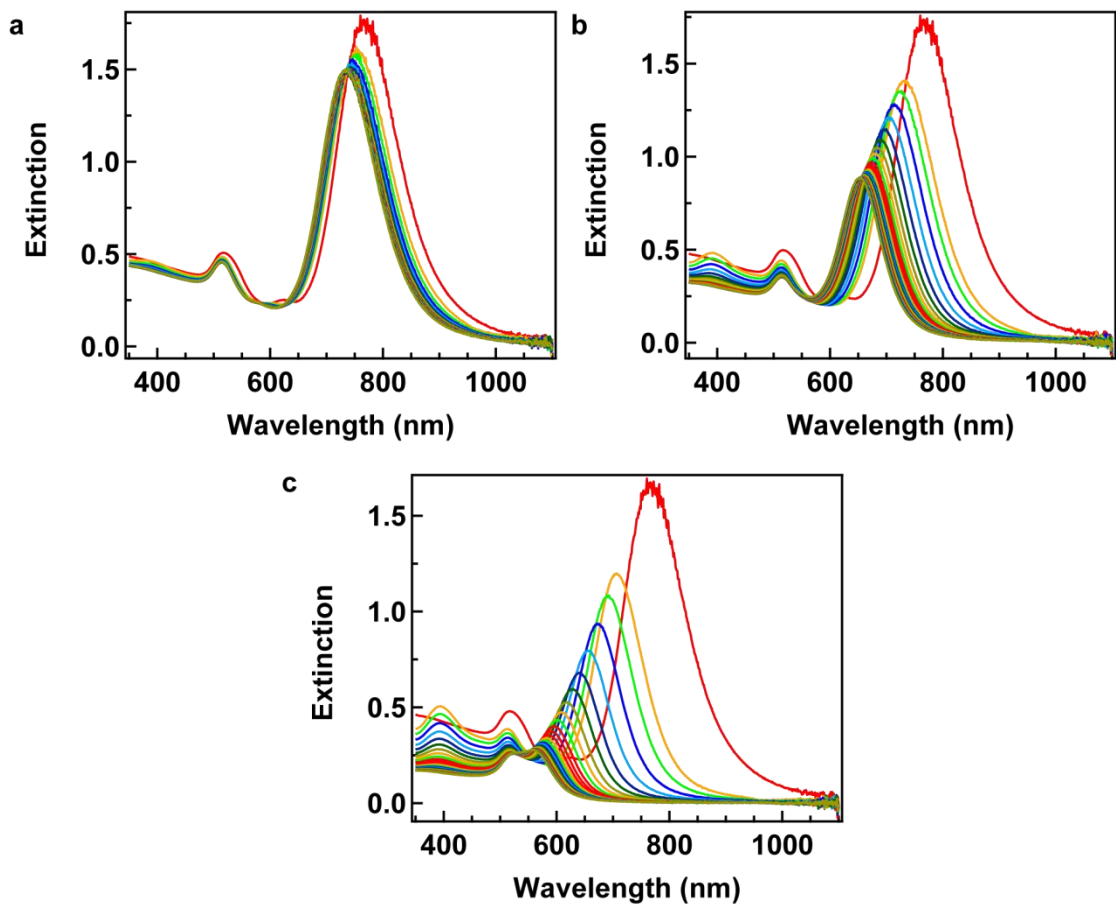


Figure S12. (a)–(c) Time evolution of the AuNR extinction spectra acquired at 0.7, 1.0, and 1.4 mM Br_2 , respectively. The spectra were recorded at 45 °C every 2 min.

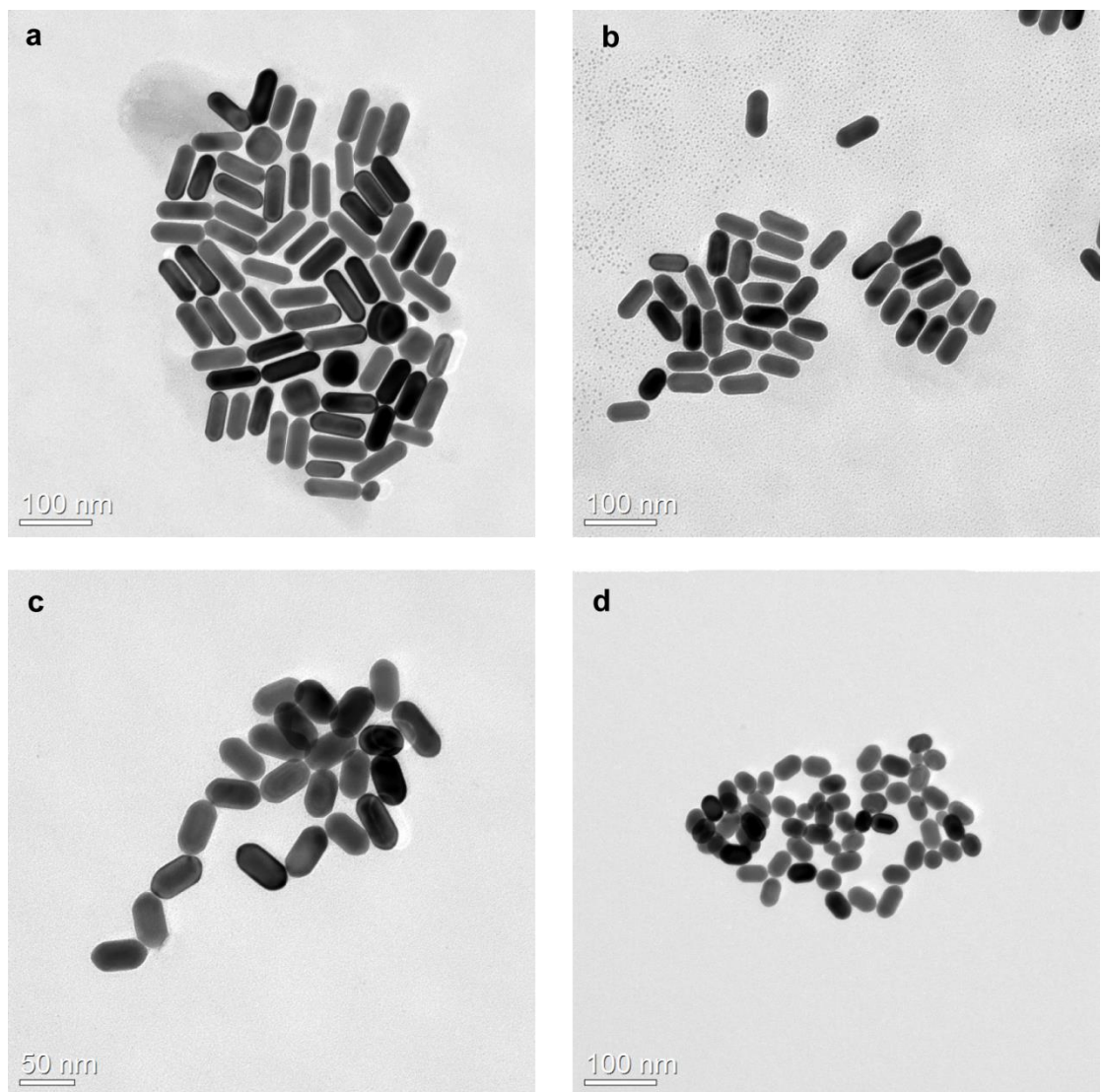


Figure S13. (a)–(d) Representative TEM images of AuNRs obtained at 0.7, 1.0, 1.2, and 1.4 mM Br_2 , respectively.